

## Supporting Information for

### Few-Layer, Large-Area, 2D Covalent Organic Framework Semiconductor Thin Films

Jeremy I. Feldblyum, Clara H. McCreery, Sean C. Andrews, Tadanori Kurosawa, Elton J. G. Santos, Vincent Duong, Lei Fang, Alexander L. Ayzner, Zhenan Bao

#### **Table of Contents**

**Section S1. Experimental Procedures.**

**Section S2. Model Compound Synthesis.**

**Section S3. Computational Modeling**

**Section S4. Pawley Refinement**

**Section S5. Discussion of Number of Molecular Layers in Thin Films**

**Section S6. Additional Supporting Data (PXRD, GI-SAXS, XAS, FTIR, PESA, Digital Photographs, AFM, UV-Vis)**

**Section S7. Transistor Mobility Calculation and Device Characteristics**

**Section S8. References**

## **Section S1. Experimental Procedures**

**Materials.** 2,6-dicarbaldehyde-4,8-dioctyloxybenzo[1,2-b:3,4-b']dithiophene (tapa, SunaTech Inc., Suzhou), tris(4-aminophenyl)amine (bdta, TCI America, Portland, OR), N,N-dimethylformamide (DMF, Fisher Scientific, Waltham, MA), MgSO<sub>4</sub> (Fisher Scientific, Waltham, MA) and glacial acetic acid (Fisher Scientific, Waltham, MA), were used as-received without further purification. N,N-diphenyl-p-phenylenediamine was synthesized as reported previously.<sup>1</sup> The synthesis of model compound **1** is described below.

**polyTB Powder Synthesis.** tapa (5.8 mg, 0.02 mmol) and bdta (15.0 mg, 0.03 mmol) were dissolved in DMF (2 mL) and acetic acid (40  $\mu$ L), aided by sonication. The solution was incubated for 24 h at 100 °C after which a bright red precipitate formed. The precipitate was washed three times over 2 days by decanting the supernatant and replacing it with fresh DMF. Where dry powder was desired, the solution was washed further by rinsing three times over 2 days with chloroform and drying under dynamic vacuum (~20 mTorr). Dry samples were stored in ambient conditions.

**polyTB Powder Synthesis for analysis by FTIR.** polyTB powder was synthesized and treated as described above, with the exception that during washing steps using DMF, DMF-powder suspensions were kept at 100 °C to ensure complete removal of any residual, soluble monomers and oligomers. However, we noted no differences between the FTIR spectra of samples washed at room temperature and those washed at 100 °C.

**polyTB Thick Film Synthesis.** tapa (5.8 mg, 0.02 mmol) and bdta (15.0 mg, 0.03 mmol) were dissolved in 3 ml DMF and 60  $\mu$ L acetic acid, aided by sonication. The solution transferred to a petri dish (3 cm dia.) in a sealed container having a saturated H<sub>2</sub>O atmosphere until a red film with a green sheen (visible by eye) had grown over the surface of the solution (typically 48-72 h). DMF was pipetted under the film to elevate it, allowing the film to be picked up from underneath with a solid substrate (glass or Si) and transferred twice in sequence to fresh DMF.

**polyTB Thin Film Synthesis.** tapa (5.8 mg, 0.02 mmol) and bdta (15.0 mg, 0.03 mmol) were dissolved in 2 ml DMF and 40  $\mu$ L acetic acid, aided by sonication. The solution was incubated for 24 h at 100 °C upon which bright red precipitate formed. The supernatant was removed from the precipitate by pipetting and filtered through P4 filter paper (Fischer Scientific, Waltham, MA) into a petri dish (3 cm dia.). The precipitate was then washed with an additional 2 mL DMF, which was subsequently filtered and added to the filtered supernatant. The petri dish was left in a sealed container having a saturated H<sub>2</sub>O atmosphere until a thin film, indicated by a green sheen, had grown over the surface of the solution (typically 48-72 h). DMF was pipetted under the film to elevate it, allowing the film to be picked up from underneath with a solid substrate (glass or Si) and transferred twice in sequence to fresh DMF. This protocol was used to prepare films for field-effect transistors.

**<sup>1</sup>H and <sup>13</sup>C NMR.** <sup>1</sup>H and <sup>13</sup>C NMR were obtained on a Varian Inova 500 MHz spectrometer. Data were analyzed with MestReNova 9.0 (Mestrelab Research S.L., Santiago de Compostela).

**FTIR Spectroscopy.** FTIR spectra were obtained using a Nicolet iS50 FTIR spectrometer (Thermo Scientific, Waltham, MA). All spectra were acquired by grazing angle ATR with a diamond prism.

**UV-Vis Spectroscopy.** UV-Vis spectra were recorded on a Cary 6000i (Agilent Technologies, Santa Clara, CA). Films were characterized in transmission mode using a standard film sample holder having a 1x1 cm<sup>2</sup> window for light transmission. Powders were analyzed using a “praying mantis” diffuse reflectance accessory. Samples were prepared by mixing 1-5% by mass of the compound of interest in a TiO<sub>2</sub> matrix and subsequently homogenizing in a mortar and pestle. Reflectance spectra were obtained using TiO<sub>2</sub> as a background. Data are reported in the form of the Kubelka-Munk equation,<sup>2</sup> which relates the diffuse scattering of light to  $k/s$  by

$$\frac{k}{s} = \frac{(1 - R)^2}{2R},$$

where  $k$  is the molar absorption coefficient,  $s$  is the scattering coefficient, and  $R$  is the absolute reflectance. In the experiment, not all reflected light is collected, so the raw data obtained during measurements are directly proportional to, but not equal to  $R$  (and by extension reported data are directly proportional to, but not equal to  $k/s$ ).

The absorption edge for all UV-Vis spectra was estimated as follows: first, the steepest portion of the spectrum at low energy (i.e., closest the HOMO-LUMO gap energy) was determined by calculating the 1<sup>st</sup> derivative of the spectrum. A line was then fit about this portion of the spectrum and the absorption edge reported as the  $x$ -intercept of this line. This approach allowed a consistent method of determining the absorption edge for all reported data and provides only an estimate of the true HOMO-LUMO gap energy.

**Powder X-ray Diffraction.** A powder sample of polyTB was packed into a 1.5 mm inner diameter Kapton capillary (Fisher Scientific, Waltham, MA), which was then sealed on both ends with epoxy (Loctite Hysol 1C, Henkel AG & Company, Düsseldorf). The sample was then mailed to beamline 11-BM of the Advanced Photon Source at Argonne National Laboratory and analyzed. A description of the instrumentation and experimental setup at 11-BM has been published,<sup>3</sup> and details may also be accessed via the Internet.<sup>4</sup>

**Grazing Incidence X-ray Scattering.** Beamline 7.3.3 at the Advanced Light Source (ALS) was used for the GISAXS experiments. Sample to detector distance (calibrated with LaB<sub>6</sub>) and X-ray energy were set at 1319.7 mm and 10 keV, respectively. Samples were measured at a grazing incidence angle of 0.12 degrees from the horizon.

**Near-Edge X-ray Absorption.** Beamline 8-2 at the Stanford Synchrotron Radiation Lightsource (SSRL) was used for angle-resolved NEXAFS experiments. Samples were deposited onto highly-doped Si substrates to prevent sample charging. Absorption intensity was collected in total electron yield mode. Spectra were normalized to the grid current of a gold foil placed

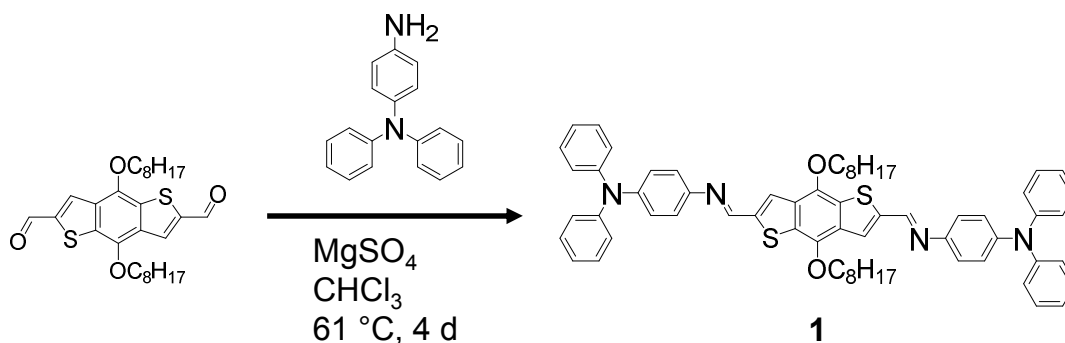
upstream of the sample, thus normalizing by the energy dependence of the photon flux. A linear pre-edge background was then subtracted, and resultant spectra were normalized to the total curve integral. The  $\pi^*$  peak intensity was then integrated, and the angular dependence of this integral was fit to a well-known equation by Stohr and Outka to determine the mean orientation of the transition dipole moment.<sup>5</sup>

**Atomic Force Microscopy.** Atomic force microscopy was performed under ambient conditions with a Veeco Multimode 3 (Veeco, Plainview, NY) in tapping mode. Data were analyzed with Gwyddion v. 2.34 (Czech Metrology Institute, Brno).

**Photoelectron Spectroscopy in Air.** Photoelectron spectroscopy in air was carried out using a Riken Keiki AC-2 photoelectron spectrometer. Films of polyTB grown using the thick film synthesis method (described above) were transferred from clean DMF to degenerately doped ( $n^{++}$ ) Si wafers and dried in air overnight under ambient conditions. Films were then analyzed with a lamp power setting of 100 nW. Data were analyzed using previously described methods.<sup>6-</sup>

**Transistor Device Fabrication and Measurement.** Degenerately doped ( $n^{++}$ ) Si wafers having 300 nm  $\text{SiO}_2$  layers were cut into  $2 \times 2 \text{ cm}^2$  substrates. Substrates were cleaned by rinsing with acetone and exposing to  $\text{O}_2$  plasma for 2 minutes under reduced pressure (200 mTorr). Immediately after cleaning, substrates were lifted beneath polyTB thin films to coat the majority of the substrate with polyTB film. Films used were of thicknesses between 5-30 nm; no correlation between film thickness and device performance was observed. 40 nm-thick Au top contacts were patterned by evaporation through a shadow mask, defining transistor channels of 50  $\mu\text{m}$  length and 4000  $\mu\text{m}$  width. Samples were analyzed with a 4200-SCS semiconductor parameter analyzer (Keithley Instruments, Inc., Cleveland, Ohio) in an inert  $\text{N}_2$  atmosphere.

## Section S2. Model Compound Synthesis.



*N,N*-diphenyl-*p*-phenylenediamine (57.2 mg, 0.22 mmol), bdta (50.0 mg, 0.10 mmol), and  $\text{MgSO}_4$  (2 g) were added to a 100 mL, 2-neck roundbottom flask. After purging with dry  $\text{N}_2$  gas for 20 minutes,  $\text{CHCl}_3$  (10 mL) was added. The resultant solution was heated to reflux while stirring under inert  $\text{N}_2$  atmosphere and held at reflux for 4 days, cooled to room temperature, and filtered to remove  $\text{MgSO}_4$ . The solvent was evaporated and the remaining solid was recrystallized from a solution of 1:5  $\text{CHCl}_3$ :hexanes (v:v) to yield compound **1** (58.1 mg, 56%) as an orange, needle-like crystal-containing powder.  $^1\text{H NMR}$  (500 MHz,  $\text{THF-}d_8$ ):  $\delta$  8.87 (s,

2H), 7.93 (s, 2H), 7.31-7.23 (m, 12H), 7.11-7.06 (m, 12H), 7.01 (tt,  $J = 7.4$  Hz, 1.1 Hz, 4H), 4.36 (t,  $J = 6.6$  Hz, 4H), 1.96-1.90 (m, 4H), 1.65-1.59 (m, 4H), 1.48-1.30 (m, 16H), 0.90 ppm (t,  $J = 7.1$  Hz, 6H).  $^{13}\text{C}$  NMR (126 MHz,  $\text{THF-}d_8$ ):  $\delta$  151.12, 147.96, 147.11, 145.46, 145.38, 144.81, 133.42, 130.46, 129.38, 125.54, 124.52, 124.10, 123.12, 122.59, 74.04, 32.12, 30.77, 29.70, 29.56, 26.27, 22.85, 13.76 ppm. HRMS (MALDI)  $m/z$   $[\text{M} + \text{H}]^+$  calcd for  $\text{C}_{64}\text{H}_{66}\text{N}_4\text{O}_2\text{S}_2$ , 987.4700, found 987.4680.

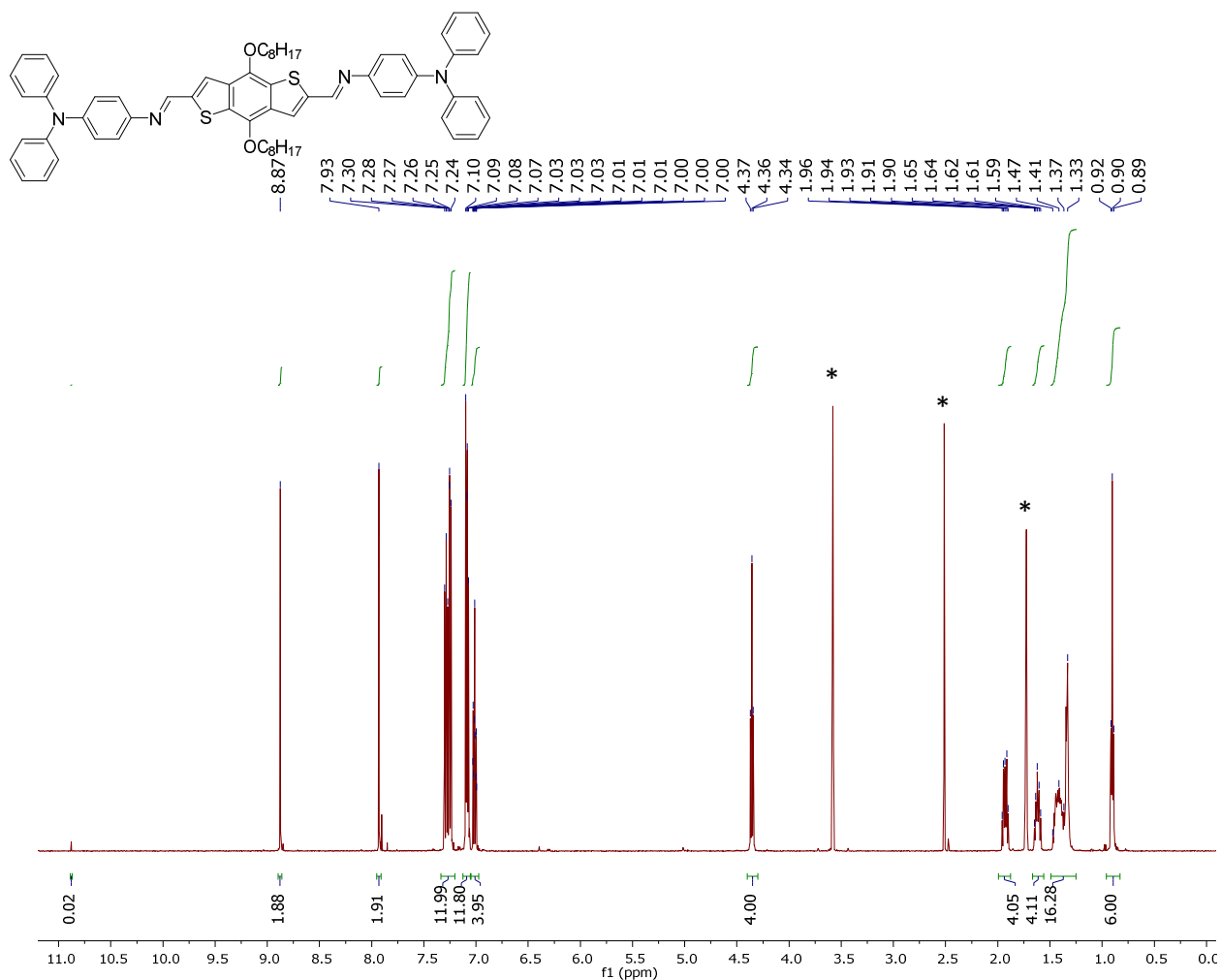


**Figure S1.**  $^1\text{H}$  NMR of model compound **1** in  $\text{THF-}d_8$  at 298 K. Asterisks denote peaks arising from solvent.

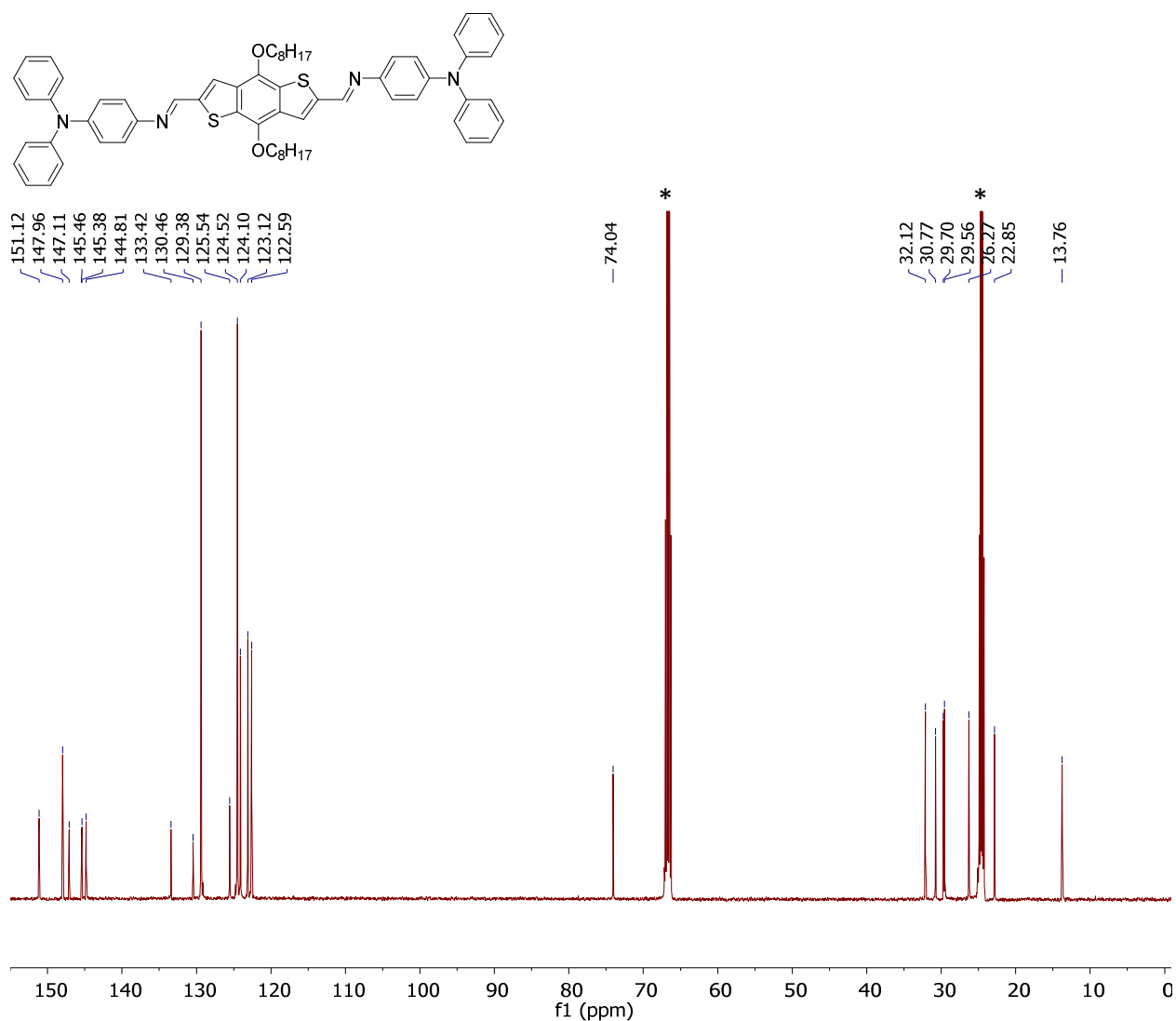


**Figure S2.** <sup>13</sup>C NMR of model compound **1** in THF-*d*<sub>8</sub> at 298 K. Asterisks denote peaks arising from solvent.

### **Section S3. Computational Modeling**

**Construction of hypothetical model of polyTB.** Using COF-5<sup>9</sup> as a template, a hexagonal-pore COF was manually constructed from bda and tapa subunits, forming a structure similar to that shown in Scheme 1 of the main text, but in the *P*1 space group, using Accelrys Materials Studio 7.0 (Biovia, San Diego, CA). The structure's geometry and unit cell parameters were then optimized using Forcite, a force field-based molecular mechanics module. For optimization, the Universal force field<sup>10</sup> was used. A “smart” algorithm was employed, which is a sequence of steepest descent, adjusted basis set Newton-Raphson, and quasi-Newton (BFGS variant) optimization algorithms. Convergence thresholds were set to  $2 \times 10^{-7}$  kcal mol<sup>-1</sup> energy change,  $1 \times 10^{-5}$  kcal mol<sup>-1</sup> Å<sup>-1</sup> maximum force,  $1 \times 10^{-3}$  GPa maximum stress, and  $1 \times 10^{-5}$  Å maximum displacement. The resulting geometry-optimized structure was used for Pawley refinement.

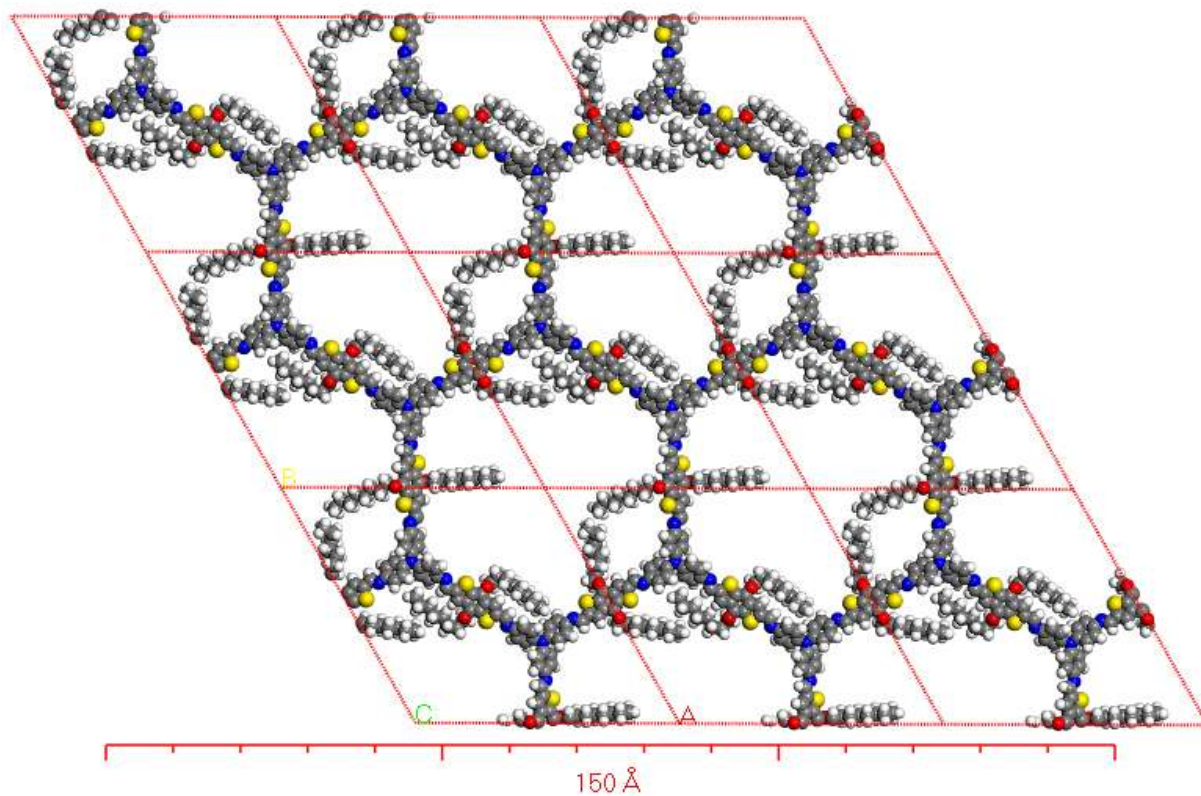


**Figure S3.** Geometry optimized, hypothetical space-filling model of a single polyTB sheet. Cell parameters:  $a = 39.271 \text{ \AA}$ ,  $b = 40.333 \text{ \AA}$ ,  $c = 4.4100 \text{ \AA}$ ,  $\alpha = 80.658^\circ$ ,  $\beta = 94.060^\circ$ ,  $\gamma = 119.893^\circ$ . Legend: H, white; C, gray; N, blue; O, red; S, yellow.

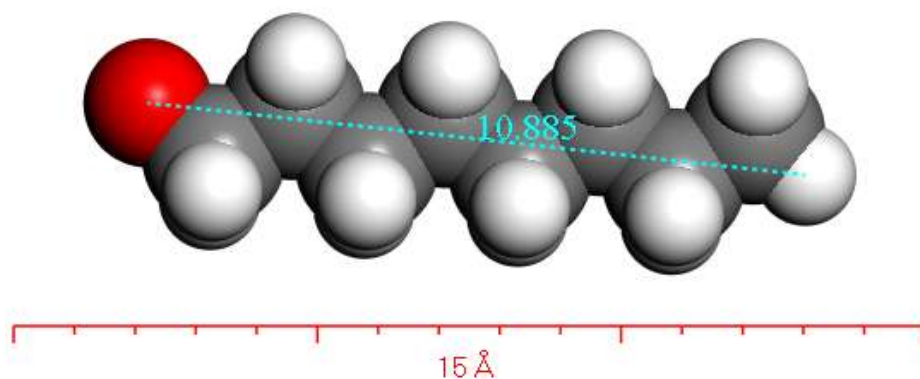


**Figure S4.** Fully extended  $-\text{OC}_3\text{H}_{17}$  chain showing chain length. The end-to-end distance is  $12.78 \text{ \AA}$  ( $10.89 \text{ \AA} + 0.69 \text{ \AA}$  (1/2 the measured bond length of the O atom to the polyTB backbone) +  $1.20 \text{ \AA}$  (the van der Waals radius of a H atom)).

#### **Section S4. Pawley Refinement**

**Pawley refinement.** Pawley refinement was carried out using the Reflex module of Accelrys Materials Studio 7.0 (Biovia, San Diego, CA). The structural model of polyTB (whose construction is described in Section S3) was used to provide starting unit cell parameters for refinement. The experimental PXRD pattern was refined from 0.5 to 3.0 in  $2\theta$  ( $\lambda = 0.413681 \text{ \AA}$ ), and peaks were fit to Pseudo-Voigt peak profiles. The fitting parameters  $U$ ,  $V$ ,  $W$  (describing peak broadening by the Caglioti equation<sup>11</sup>),  $NA$ , and  $NB$  (profile parameters, which describe peak shape angle dependence), and line shift parameters according to the equation  $2\theta_{\text{corrected}} = 2\theta_{\text{measured}} + T_0 + T_1\cos(\theta) + T_2\sin(2\theta)$ , where  $T_0$  is the zero point (accounting for sample displacement, in degrees  $2\theta$ ),  $T_1$  is the absorption parameter (in degrees  $2\theta$ ), and  $T_2$  is the eccentricity parameter (in degrees  $2\theta$ ), and unit cell parameters  $a$ ,  $b$ ,  $c$ ,  $\alpha$ ,  $\beta$ , and  $\gamma$ , were used as freely varying parameters for refinement. A 20-order polynomial was used to model the experimental background. No corrections were made for peak asymmetry or broadening due to crystallite size, lattice strain, or preferred orientation. The  $2\theta$  range used for refinement did not incorporate any reflections including the  $(0\ 0\ l)$  plane as the  $(001)$  reflection was exceptionally broad, indicating a relative lack of order along the crystallographic  $c$ -axis (Figure S5). Refined cell parameters:  $a = 40.1432 \text{ \AA}$ ,  $b = 39.2727 \text{ \AA}$ ,  $c = 4.2545 \text{ \AA}$ ,  $\alpha = 98.5871^\circ$ ,  $\beta = 89.6562^\circ$ ,  $\gamma = 122.1216^\circ$ .

#### **Section S5. Discussion of Number of Molecular Layers in Thin Films**

AFM data (Figures 3b and S12) show that thin polyTB films grown as described in Section S1, “polyTB Thin Film Synthesis,” grow in layers of 1.8 nm thickness. While this is thicker than would be expected for an atomically thin sheet, we explore here the possibility that these films could still contain one or two molecular layers. In the former case (single molecular layers), the alkyl chains originating from bdta-derived subunits might extend both above and below the plane of the polyTB sheet. Such alkyl chain extension is reasonable considering the high polarity of the film growth medium and the preferential growth of the film at the solution-air interface, and that a fully extended  $\text{OC}_8\text{H}_{17}$  group is approximately 1.3 nm in length (Figure S4). Alkyl chains oriented above and below the plane of the COF sheet could be interdigitated or close-packed; the porous structure (and hence, low density of alkyl chains) of the idealized polyTB model (and agreement of PXRD data with this model) would suggest that alkyl chains between layers might indeed be interdigitated. Were layers composed of two molecular sheets, alkyl chains could be oriented above and below the individual sheets for the top and bottom sheets, respectively (again, with the possibility interdigitation between alkyl chains).

Attempts to characterize these films by transmission electron microscopy (TEM) resulted in rapid degradation under electron beam irradiation.



**Section S6. Additional Supporting Data (PXR, GI-SAXS, XAS, FTIR, PESA, Digital Photographs, AFM, UV-Vis)**

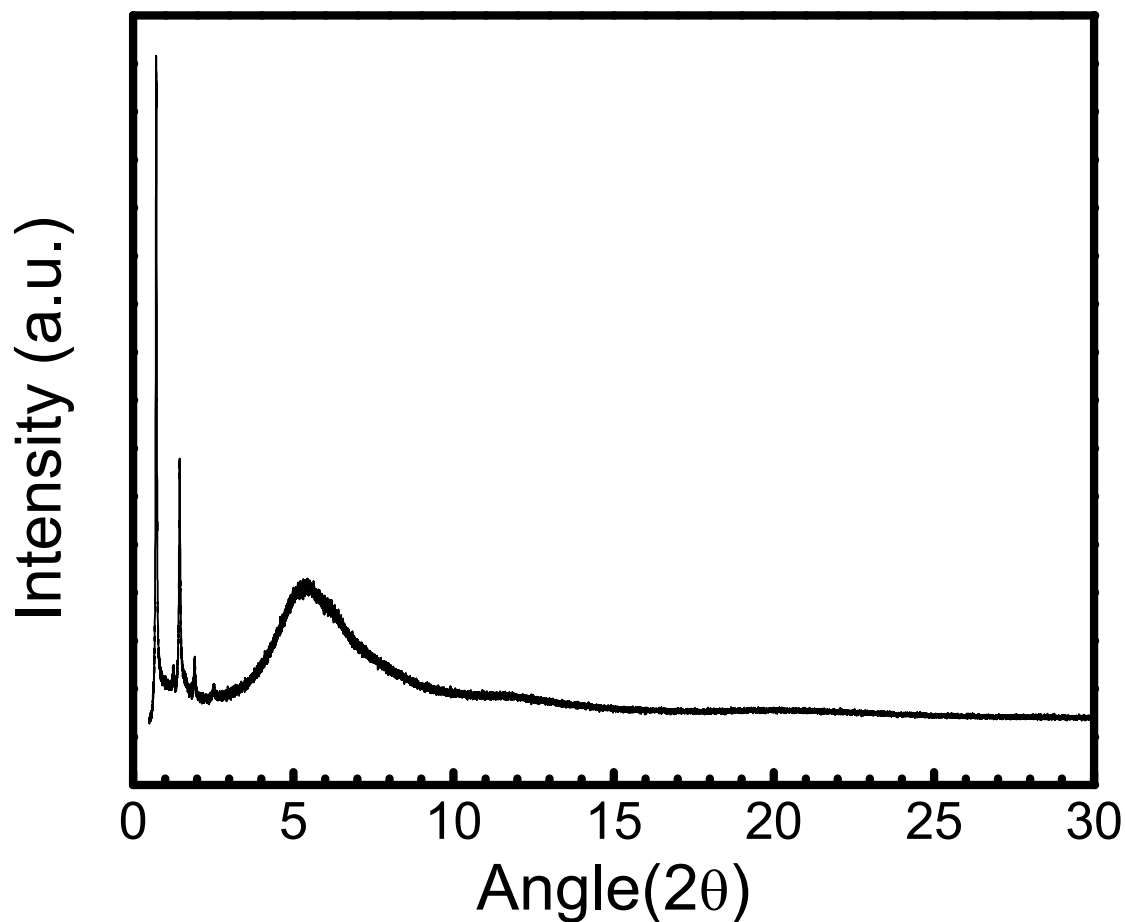


**Figure S5.** Complete PXR pattern of polyTB powder. The broad feature from  $\sim 4.5$ -8 in  $2\theta$  is ascribed to a broad distribution of repeat distances along the crystal system  $c$ -axis, suggesting a non-uniform distribution of sheet-to-sheet distances. ( $\lambda = 0.413681 \text{ \AA}$ , synchrotron radiation)

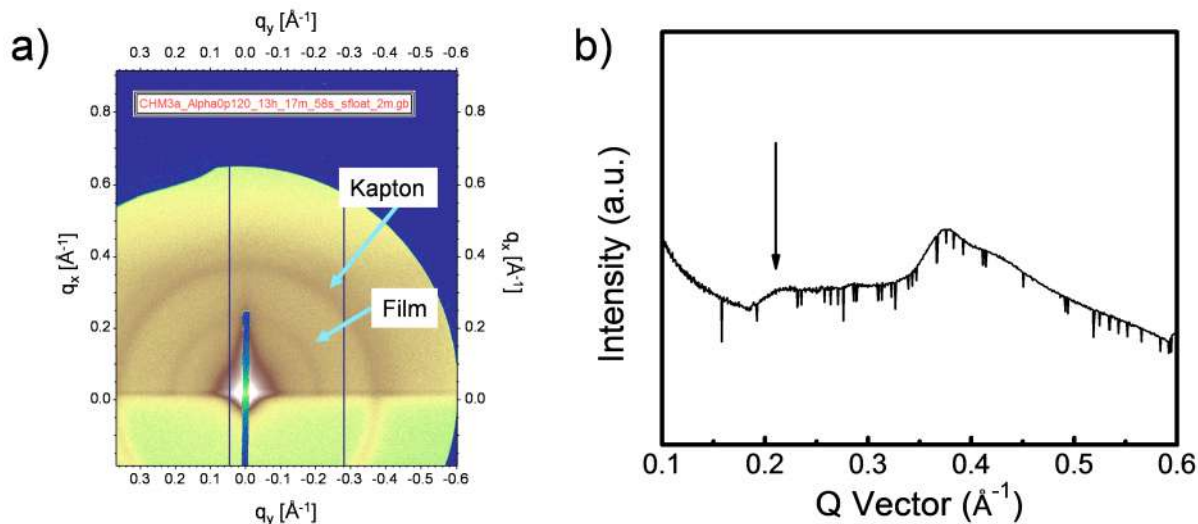


**Figure S6.** a) 2D scattering image showing a weak peak at  $0.218 \text{ \AA}^{-1}$ , corresponding to a  $d$ -spacing of  $28.8 \text{ \AA}$ . b) Intensity profile summed over all angles for a given  $q$  showing onset of the COF peak (indicated by the black arrow). The peak at  $Q \sim 0.37 \text{ \AA}^{-1}$  originates from the Kapton substrate.

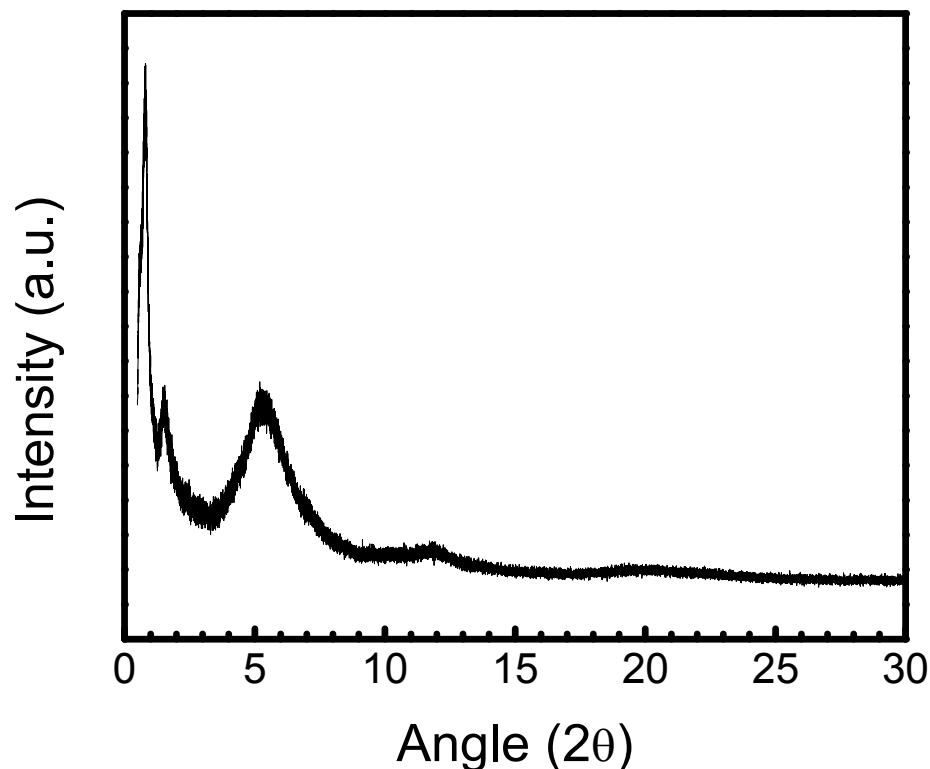


**Figure S7.** PXRD pattern of dry polyTB powder. Crystallinity is severely reduced after drying. The  $2\theta$  value for the most intense peak is  $0.798$  ( $Q = 0.211 \text{ \AA}^{-1}$ ). ( $\lambda = 0.413901 \text{ \AA}$ , synchrotron radiation).

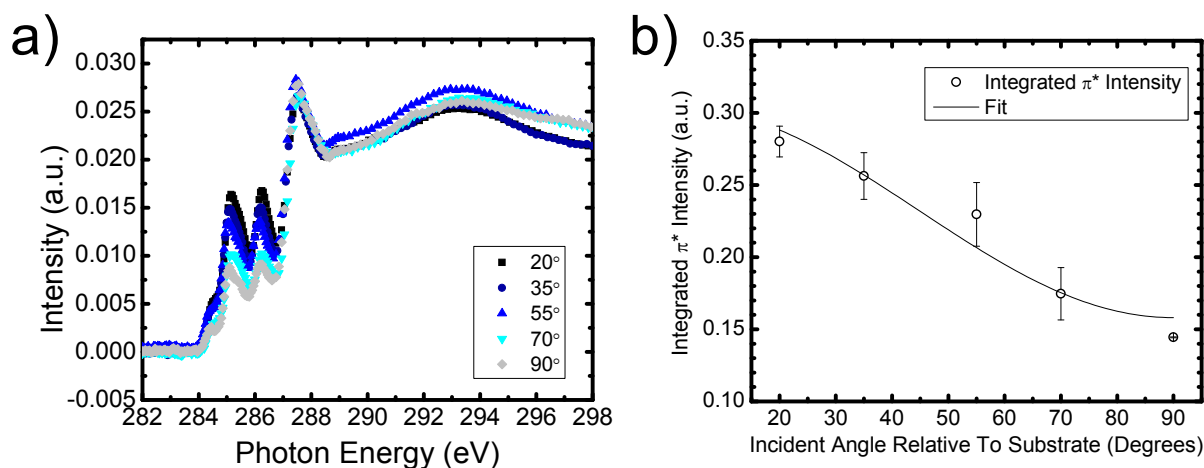


**Figure S8.** a) Angle-resolved C K-edge near-edge X-ray absorption spectra of a thick polyTB film deposited on a Si wafer.  $\pi^*$  peaks are present at approximately 285-286.5 eV. b) Measured (integrated)  $\pi^*$  intensities are fit to equation 9.16a in reference 12 to determine the tilt angle of the transition dipole moment with respect to the substrate. An average tilt angle of  $50.5^\circ$  was calculated, corresponding to a tilt of  $39^\circ$  with respect to the substrate for the p component of unoccupied molecular orbitals in the COF backbone (for example, bdtA-based subunits and phenyl rings in the tapa-based subunits). While these data suggests only a weak preferred orientation with respect to the substrate, we note that even for COF layers perfectly parallel with respect to the substrate,  $sp^2$ -hybridized components of the COF backbone are likely tilted due to sterics. For example, in our computational model (Figure S3), phenyl ring components of the tapa-derived subunits are tilted an average of  $35.5 \pm 3.3^\circ$  relative to the plane of the polymer sheet. Hence, while the preferred orientation is weak, it is still significant (a purely isotropic sample would result in an average tilt of  $45^\circ$  with respect to the substrate).

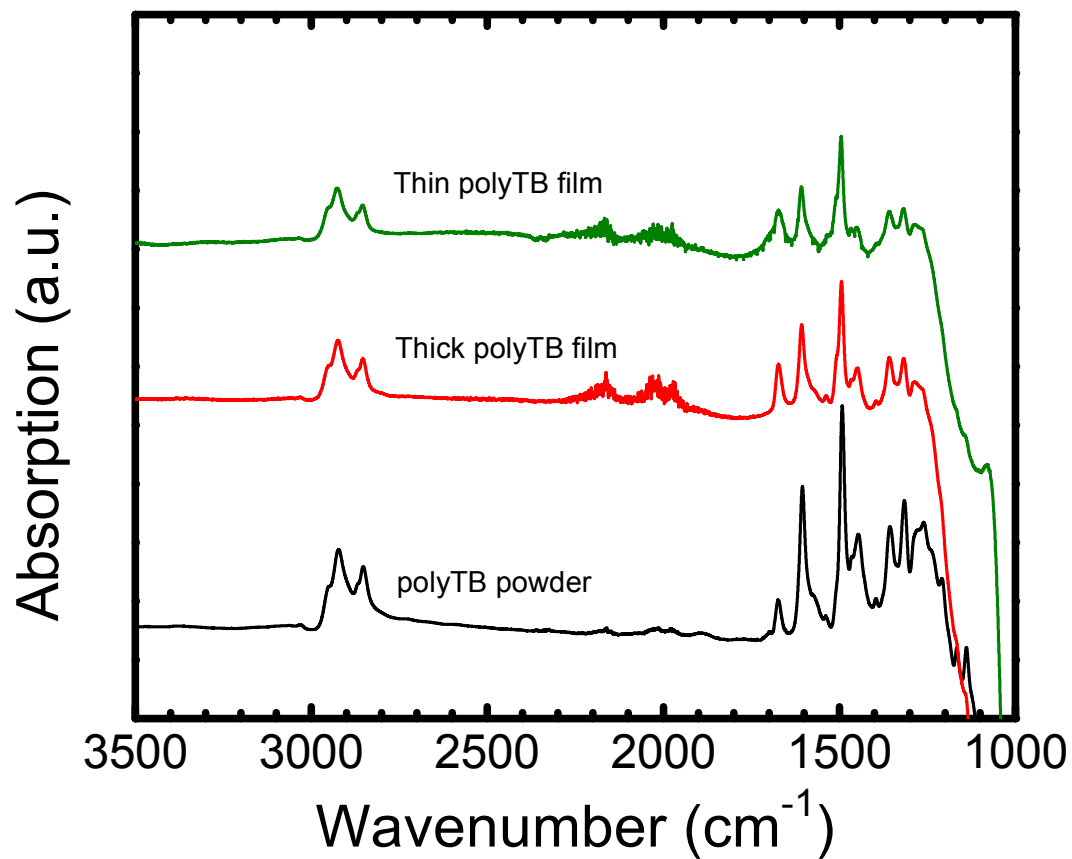


**Figure S9.** ATR-FTIR data comparing the infrared absorption characteristics of polyTB thick and thin films with those of polyTB powder. Data are offset along the y-axis for clarity.

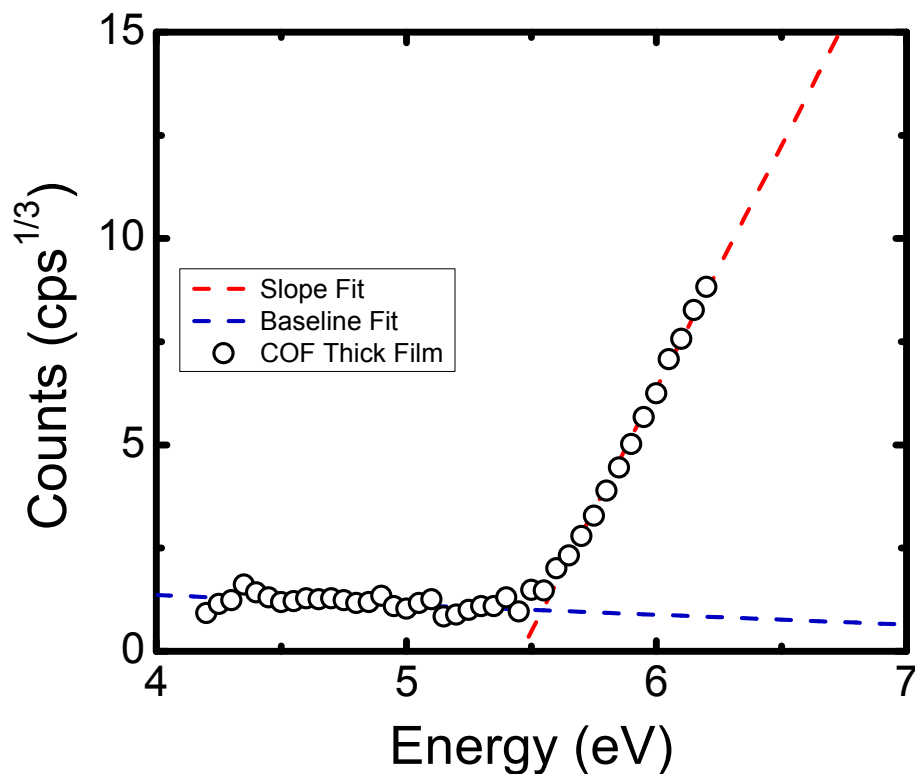


**Figure S10.** Representative photoelectron spectroscopy in air (PESA) analysis of a COF film synthesized via the thick film route. An average HOMO level of 5.5 eV was determined over three samples measured (measured HOMO levels were consistent over all three samples). A LUMO of 3.5 eV can be estimated from the experimentally determined HOMO level and the band gap (2.0 eV) estimated from electronic spectroscopy.

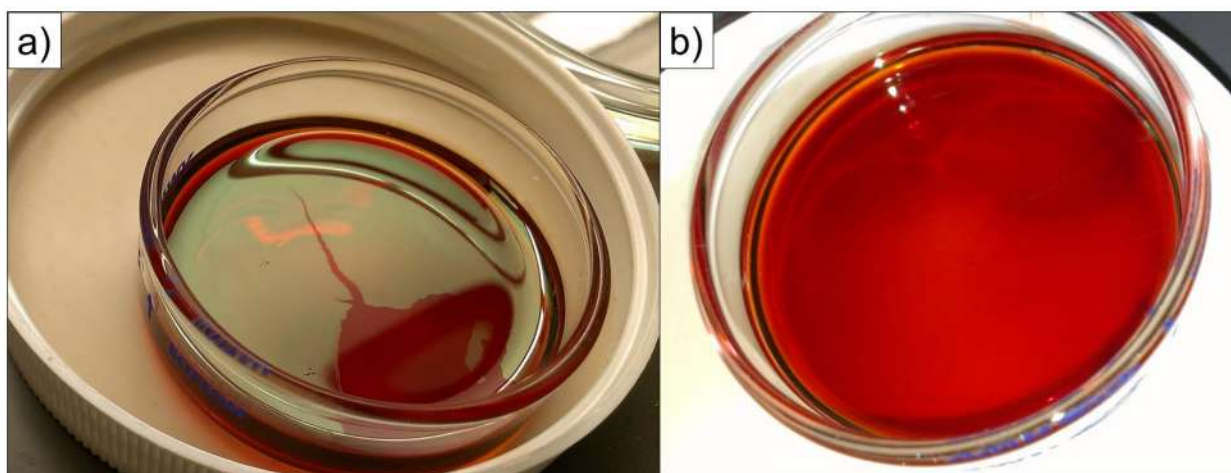


**Figure S11.** a) Photograph of a thin polyTB film in its original growth medium after one section was lifted out. The film is visible as the lighter green-tinted portion of the surface of the red solution. During transfer, a crack formed in the film. b) Photograph of the same film from a different angle where the film is only very faintly visible as a slightly darker red region on the solution surface.

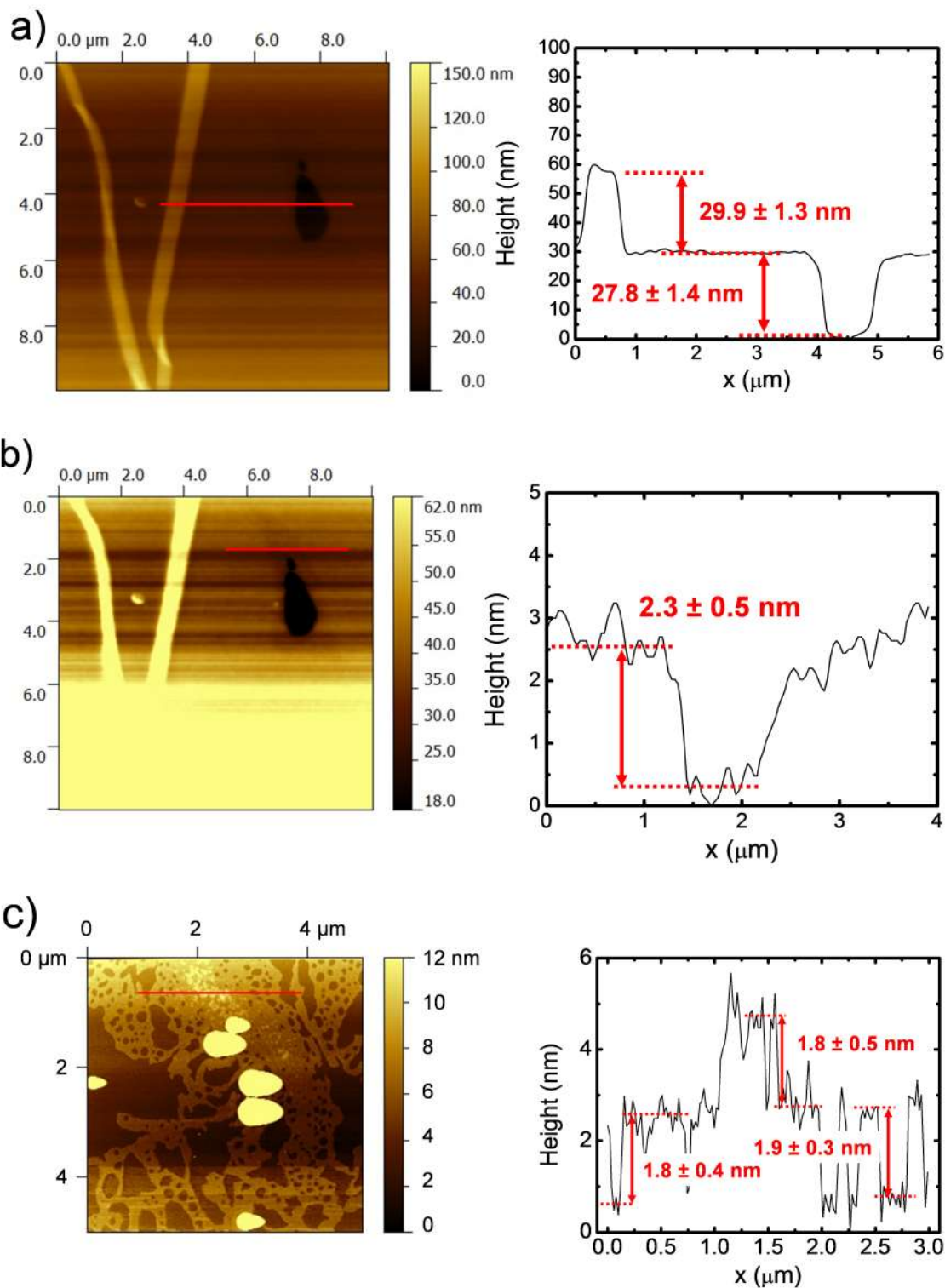


**Figure S12.** a) Thickest of thin polyTB films synthesized for this work. b) The same AFM image as shown in part (a) with a finer height scale to aid visualizing the area where two layers within the film are visible. c) Thin polyTB film showing the beginnings of growth of a subsequent layer.

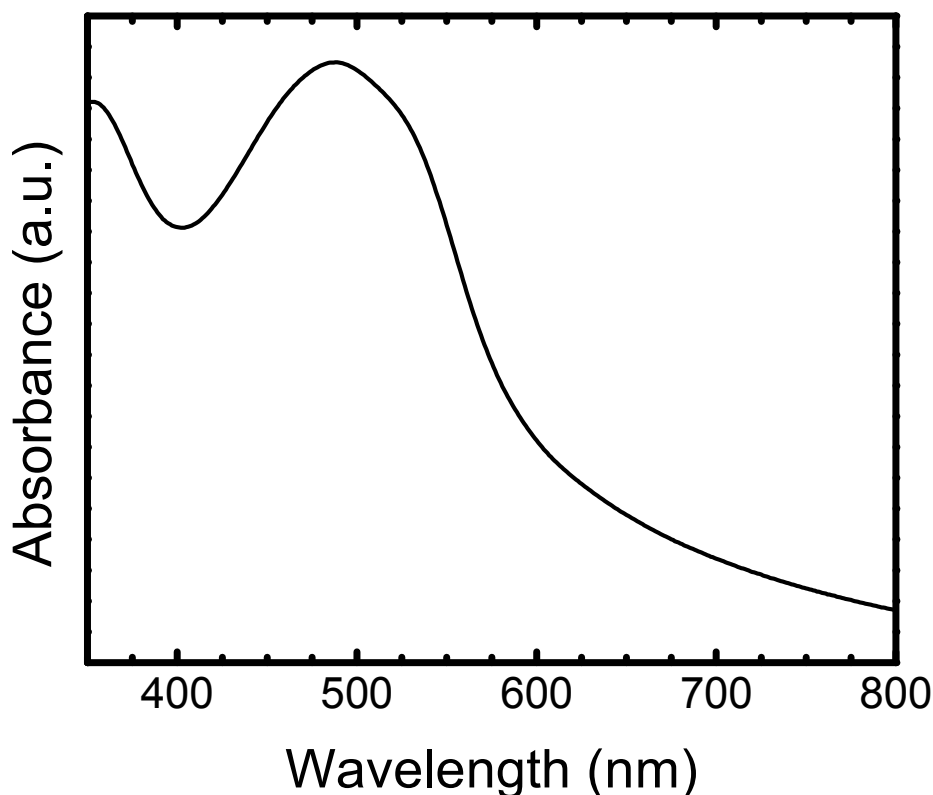


**Figure S13.** UV-Vis spectrum of polyTB thin film on a glass microscope slide. The absorption edge (see Section S1) is 614 nm (2.0 eV).

**Video S1.** Video showing as-synthesized thick polyTB film manipulated by tweezers. Available as online supporting information at <http://pubs.rsc.org/en/journals/journalissues/cc>.

**Video S2.** Video showing as-synthesized thick polyTB film transferred from original growth medium to a new petri dish filled with DMF. Available as online supporting information at <http://pubs.rsc.org/en/journals/journalissues/cc>.

### **Section S7. Transistor Mobility Calculation and Device Characteristics**

Mobility  $\mu$  was calculated from the forward sweep in the linear regime ( $\mu_{\text{lin}}$ ) of transistor transfer plots ( $I_{\text{SD}}$  vs.  $V_{\text{G}}$ ), by the equation<sup>13</sup>

$$I_{\text{SD}} = \mu_{\text{lin}} \frac{W}{L} C_i (V_{\text{G}} - V_{\text{T}}) V_{\text{SD}},$$

where  $I_{\text{SD}}$  is the source-drain current,  $W$  and  $L$  are the width and length of the channel (4000  $\mu\text{m}$  and 50  $\mu\text{m}$ , respectively),  $C_i$  is the gate dielectric capacitance (11.5  $\text{nF}/\text{cm}^2$ ),  $V_{\text{G}}$  is the gate voltage,  $V_{\text{T}}$  is the threshold voltage, and  $V_{\text{SD}}$  is the source-drain voltage (held at -100 V for our experiments). Mobility in the saturation regime ( $\mu_{\text{sat}}$ ) was calculated<sup>13</sup> by

$$I_{SD} = \mu_{sat} \frac{W}{L} C_i (V_G - V_T)^2.$$

Measurements of device properties for all devices are shown in Table S1 below. We note that no ambipolar character was measured for any devices (all operated solely as p-type devices).

Device Number	$\mu_{lin}$ (cm <sup>2</sup> V <sup>-1</sup> s <sup>-1</sup> )	$\mu_{sat}$ (cm <sup>2</sup> V <sup>-1</sup> s <sup>-1</sup> )	on/off ratio	$V_T$ (V)
1	$5.75 \times 10^{-6}$	$6.06 \times 10^{-6}$	144	-40
2	$5.23 \times 10^{-6}$	$1.15 \times 10^{-5}$	900	-66
3	$4.95 \times 10^{-6}$	$5.87 \times 10^{-6}$	2950	-47
4	$3.63 \times 10^{-6}$	$4.06 \times 10^{-6}$	1230	-43
5	$3.49 \times 10^{-6}$	$5.06 \times 10^{-6}$	1890	-53
6	$1.32 \times 10^{-6}$	$2.59 \times 10^{-6}$	342	-62
7	$2.95 \times 10^{-6}$	$5.97 \times 10^{-6}$	507	-62
8	$2.84 \times 10^{-6}$	$4.50 \times 10^{-6}$	183	-56
9	$2.90 \times 10^{-6}$	$3.14 \times 10^{-6}$	2160	-41
10	$1.16 \times 10^{-6}$	$1.39 \times 10^{-6}$	509	-45
11	$1.26 \times 10^{-6}$	$1.64 \times 10^{-6}$	515	-49
12	$1.47 \times 10^{-6}$	$1.83 \times 10^{-6}$	459	-47
13	$2.53 \times 10^{-6}$	$8.17 \times 10^{-6}$	302	-70
14	$3.56 \times 10^{-6}$	$8.65 \times 10^{-6}$	785	-60
15	$1.56 \times 10^{-6}$	$1.21 \times 10^{-6}$	251	-30
16	$9.00 \times 10^{-7}$	$1.28 \times 10^{-6}$	440	-50
Average	$(3.0 \pm 1.5) \times 10^{-6}$	$(3.9 \pm 2.5) \times 10^{-6}$	$850 \pm 810$	$-51 \pm 11$

**Table S1.** polyTB thin film transistor device characteristics. Reported errors represent one standard deviation from the mean.

Transfer (Figure S14a) and output (Figure S14b) plots are shown below for a typical polyTB transistor. The transfer plot shows significantly lower back sweep current. Such hysteresis can be caused by the presence of deep majority carrier traps or mobile ions (reasonable considering initial exposure of films to acidic conditions during synthesis).<sup>14</sup> Device degradation may also play a significant role, consistent with a reduction in absolute current with increasing  $V_{SD}$  in the output plot for  $V_G = -60, -80,$  and  $-100$  V after saturation appears to be reached. This effect may also mask where the device reaches “true” saturation as the reduction in current due to degradation may be greater in magnitude than the increase in current due to increasing  $V_{SD}$ .



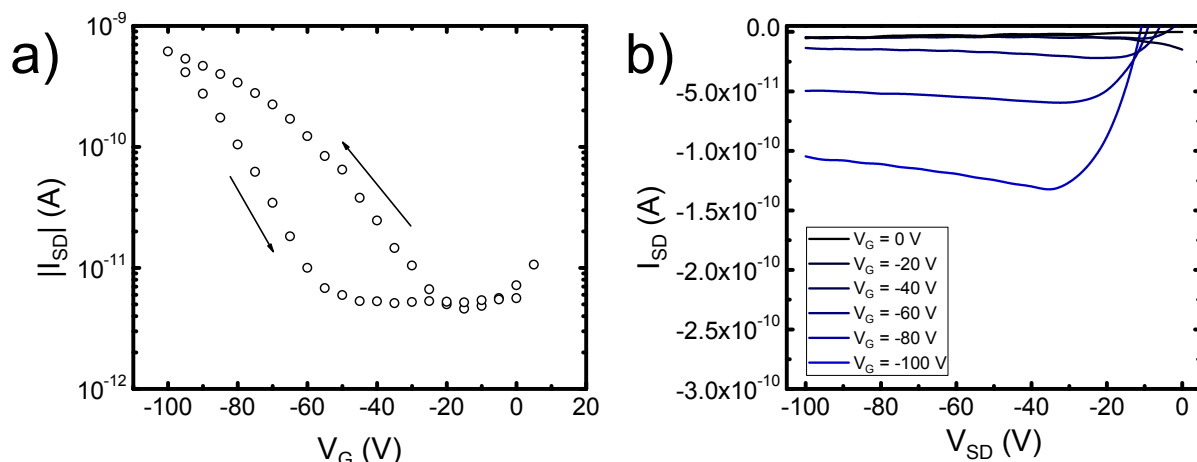


**Figure S14.** a) Transfer plot of a typical polyTB transistor, showing hysteresis. b) Output plot of a typical polyTB transistor.

Among the reasons for the relatively low mobility of our devices (discussed in the main text), we believe grain boundaries may play a significant role. To estimate the number of grain boundaries charge carriers must traverse in between the source and drain electrodes, we used the Scherrer equation<sup>15</sup> to estimate the grain size of crystallites in bulk powder polyTB. A (lateral) crystallite diameter of 65.7 nm was determined, which would correspond to 761 grain boundaries between source and drain electrodes 50  $\mu\text{m}$  apart. Assuming polyTB films do not contain larger crystalline domains than polyTB bulk powder when grown, this calculation then represents a lower limit for the number of grain boundaries between source and drain electrodes. Furthermore, since the crystallinity of the polyTB films used for transistors is reduced when films dry, there may be appreciably large amorphous domains in between crystalline regions, further contributing to a reduction in mobility.

## Section S8. References

- (1) Lee, W.-Y.; Kurosawa, T.; Lin, S.-T.; Higashihara, T.; Ueda, M.; Chen, W.-C. *Chem. Mater.* **2011**, *23*, 4487.
- (2) Kubelka, P. *J. Opt. Soc. Am.* **1948**, *38*, 448.
- (3) Wang, J.; Toby, B. H.; Lee, P. L.; Ribaud, L.; Antao, S. M.; Kurtz, C.; Ramanathan, M.; Von Dreele, R. B.; Beno, M. A. *Rev. Sci. Instrum.* **2008**, *79*.
- (4) Description of Beamline 11-BM at Argonne National Laboratory. <http://11bm.xray.aps.anl.gov/documents/11BMdescription2page.pdf>. Accessed February 6, 2015.
- (5) Stöhr, J.; Outka, D. A. *Phys. Rev. B* **1987**, *36*, 7891.
- (6) Photoelectron Spectroscopy - RKI Instruments. [www.rkiinstruments.com/pdf/AC2.pdf](http://www.rkiinstruments.com/pdf/AC2.pdf). Accessed July 6, 2015.
- (7) Kirihata, H.; Uda, M. *Rev. Sci. Instrum.* **1981**, *52*, 68.
- (8) Sano, T.; Hamada, Y.; Shibata, K. *IEEE J. Quantum Electron.* **1998**, *4*, 34.
- (9) Côté, A. P.; Benin, A. I.; Ockwig, N. W.; O'Keeffe, M.; Matzger, A. J.; Yaghi, O. M. *Science* **2005**, *310*, 1166.
- (10) Rappe, A. K.; Casewit, C. J.; Colwell, K. S.; Goddard, W. A.; Skiff, W. M. *J. Am. Chem. Soc.* **1992**, *114*, 10024.
- (11) Caglioti, G.; Paoletti, A.; Ricci, F. P. *Nucl. Instrum.* **1958**, *3*, 223.
- (12) Stöhr, J. *NEXAFS Spectroscopy*; Springer: Berlin, 1996.

- (13) Siringhaus, H. *Adv. Mater.* **2014**, 26, 1319.
- (14) Egginger, M.; Bauer, S.; Schwödiauer, R.; Neugebauer, H.; Sariciftci, N. S. *Monatsh. Chem.* **2009**, 140, 735.
- (15) Scherrer, P. *Göttinger Nachrichten Math. Phys.* **1918**, 2, 98.